Research on Dynamical Characteristics of an Eccentric Rotor System

Xichen Hou [1*], Zhiyong Yin [1], Leipeng Song [2], Jiedong Shi [2]

[1]National Key Laboratory of Ship Vibration & Noise, China Ship Science Research Center, Wuxi, Jiangsu, 214082, China
[2]State Key Laboratory of Mechanics and Control of Mechanical Structures, Nanjing University of Aeronautics and Astronautics, Nanjing, Jiangsu, 210016, China

*Corresponding email: 260235440@qq.com

Abstract. Vibration and noise caused by the eccentric rotor system in operation seriously affect the safety of equipment, so it is necessary to study the dynamic characteristics of the eccentric rotor system. In this paper, the dynamic theoretical model of the eccentric rotor is established based on the Timoshenko beam-shaft theory, and the dynamic characteristics of the eccentric rotor system under different rotate speeds are analyzed by the finite element method. Results show that the vibration of the eccentric rotor system is significantly correlated with the mode and dominant frequency of the rotor system. When the speed of the accelerated eccentric rotor system is close to the critical speed, the resonance between rotation and precession will occur, and the vibration amplitude of the rotor system will increase significantly.

Keywords: eccentric rotor system, Timoshenko beam-shaft theory, rotation speed, finite element method

1 Introduction

Rotating machinery, as the most crucial power equipment in modern industry, is extensively utilized in sectors such as aerospace, maritime, automotive, and energy [1-3]. In the shipping industry, rotating machinery is widely utilized in auxiliary devices such as engines, pumps, and blowers. Due to high temperatures, high speeds, and heavy loads, the rotor system of rotating machinery may experience deformation, wear, and changes in concentricity. These factors can cause the rotor's center of mass to deviate from the rotating center and result in vibration, leading to unnecessary harm [4-5].

Currently, many references have studied the dynamic characteristics of eccentric rotor systems. Zhu et al. studied the effect of eccentricity on the dynamic characteristics of turbocharger rotor systems and found that under small eccentricity [6], the rotor system would experience oil film instability at lower speeds, and increasing eccentricity would improve rotor stability. Xiang et al. established a dynamic model of the nonlinear rotor-bearing-seal coupling system, and studied its nonlinear dynamic behavior under different eccentricity values [7]. Yuan et al. found in their study on the influence of mass

A. S. B. A Rashid et al. (eds.), *Proceedings of the 2024 3rd International Conference on Applied Mechanics and Engineering Structures (AMES 2024)*, Advances in Engineering Research 34,
https://doi.org/10.2991/978-94-6463-473-0_16

eccentricity on the dynamic response of rotor systems that the amplitude of the rotor system increases as the eccentric mass and eccentric distance increase [8]. Shao et al. also found that the system response is larger when the eccentric mass is larger in their study on the influence of mass eccentricity on the vibration characteristics of cracked rotor systems. Ma et al. established a full-free-degree helical gear dynamics model and coupled it with the finite element model of the rotor system to analyze the vibration characteristics of the helical gear coupled rotor system with geometric eccentricity.

Based on the existing literature, it is evident that current research primarily focuses on analyzing the vibration response of rotor systems with eccentricity and eccentric mass. However, there is a lack of research on the influence of rotational speed on the dynamic response of eccentric rotor systems. This study analyzed the vibration response of a single-span rotor system under different speed conditions using COMSOL Multiphysics software.

2 Single-Disc Asymmetric Offset Rotor System Dynamics Model

Taking the rigid supported single-disc symmetric eccentric rotor system as an example, the Timoshenko beam shaft model is used to model and analyze the dynamic characteristics of the shaft, as shown in Fig. 1 (a). The rotor system has an equal cross-section circular shaft, and both ends are supported by two identical bearings δ. A and B are two elastic supports at both ends, and O is the center of the disk. The length of the AO section is set as l_1 and the length of the OB section as l_2, as shown in Fig. 1 (b). The stiffness at both ends is k_1 and k_2, respectively. Considering the rotational axis with dynamic symmetry in the cross-section, we set the beam axis direction as the z-axis, the neutral axis deformation curves as $x(z, t)$ and $y(z, t)$, and the section rotation angle as $\theta_x(z, t)$ and $\theta_y(z, t)$. Cutting the microsegment of the axis, the displacement of the centroid of this microsegment is $x = x(z, t)$, $y = y(z, t)$, the deflection angle is $\theta_x = \theta_x(z, t)$, $\theta_y = \theta_y(z, t)$, and the force state of the rotating axis section is shown in Fig. 1(c).

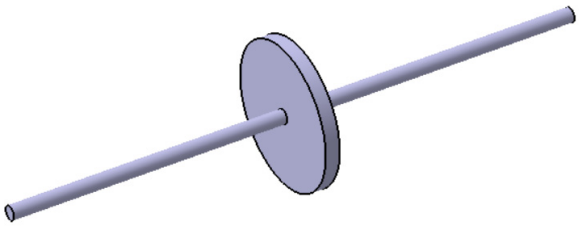

(a) Eccentric rotor system with symmetric rigid supported single disc

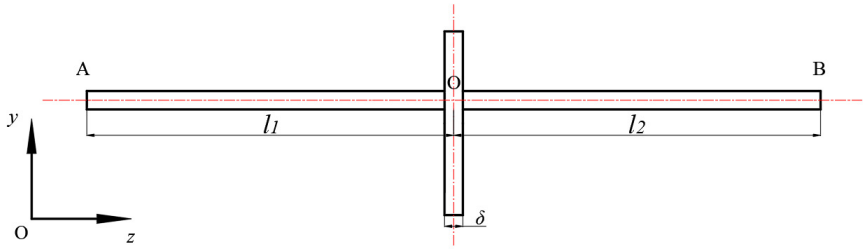

(b) Geometric parameters of the rotor system

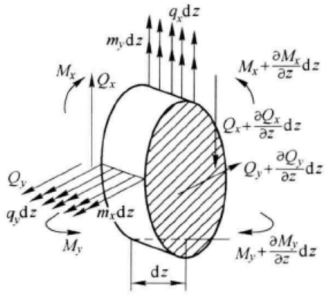

(c) Force analysis of spindle microsegment

Fig. 1. Dynamic model of a single disc symmetric eccentric rotor system

The differential equation for the axis of rotation is

$$\begin{cases} \rho A\ddot{x} = -\frac{\partial Q_x}{\partial z} + q_x \\ \rho A\ddot{y} = -\frac{\partial Q_y}{\partial z} + q_y \\ \rho I\ddot{\theta}_x + 2\Omega\rho\dot{\theta}_y = \frac{\partial M_x}{\partial z} - Q_x + m_x \\ \rho I\ddot{\theta}_y - 2\Omega\rho I\dot{\theta}_x = \frac{\partial M_y}{\partial z} - Q_y + m_y \end{cases} \tag{1}$$

In the equation, I represents the sectional moment of inertia; q_x and q_y represent the distributed external loads; m_x and m_y are distributed torque; M_x and M_y are bending moments; Q_x and Q_y are shear forces. Let$r = x + iy, \theta = \theta_x + i\theta_y, M = M_x + iM_y, Q = Q_x + iQ_y, q = q_x + iq_y, m = m_x + im_y$, then Equation (1) can be condensed into the following complex form:

$$\begin{cases} \rho A\bar{r} = -\frac{\partial Q}{\partial z} + q \\ \rho I\theta - 2\Omega\rho \mathrm{I}i\theta = \frac{\partial M}{\partial z} - Q + m \end{cases} \tag{2}$$

Eliminating the shear force Q, we get:

$$\frac{\partial}{\partial z}(\rho I\ddot{\theta} - 2\Omega\rho Ii\dot{\theta}) = \frac{\partial^2 M}{\partial z^2} + \frac{\partial m}{\partial z} + \rho A\ddot{r} - q \tag{3}$$

For the Timoshenko beam-axle system, its constitutive relationship and displacement compatibility conditions can be expressed by the following formula:

$$M = EI\frac{\partial\theta}{\partial z}, \theta = \frac{\partial r}{\partial z} + \frac{Q}{\mu AG} \tag{4}$$

In this equation, G represents the shear modulus, and $G = E/2(1+v)$G, where E is the modulus of elasticity and v is the Poisson's ratio; μ is the shear coefficient of the cross-section, which is determined by the geometry of the cross-section, and its value is generally between 0.45 and 0.9, with μ =0.5 for thin-walled circular cross-sections and μ=0.9 for solid circular cross-sections. Substituting Equation (4) into Equation (2) yields

$$\begin{cases} \rho A\ddot{r} + \frac{\partial}{\partial z}\left[\mu AG\left(\theta - \frac{\partial r}{\partial z}\right)\right] = q \\ \rho I\ddot{\theta} - 2\Omega\rho I\dot{\theta} = \frac{\partial}{\partial z}\left(EI\frac{\partial\theta}{\partial z}\right) - \mu AG\left(\theta - \frac{\partial r}{\partial z}\right) + m \end{cases} \tag{5}$$

For a uniform cross-section shaft, the cross-section parameters are independent of z, as shown by the first equation in Equation (5).

$$\frac{\partial\theta}{\partial z} = \frac{\partial^2 r}{\partial z^2} + \frac{1}{\mu AG}(q - \rho A\ddot{r}) \tag{6}$$

By combining Equations (5) and (6), it can be concluded that:

$$\begin{aligned} &\frac{\partial^4 r}{\partial z^4} - \frac{\rho}{E}\left(1 + \frac{E}{\mu G}\right)\frac{\partial^4 r}{\partial z^2\,\partial t^2} + \frac{2\Omega\rho i}{E}\frac{\partial^3 r}{\partial z^2\,\partial t} + \frac{\rho A}{EI}\frac{\partial^2 r}{\partial t^2} \\ &\quad - \frac{2\Omega\rho^2 i}{\mu EG}\frac{\partial^3 r}{\partial t^3} + \frac{\rho^2}{E\mu G}\frac{\partial^4 r}{\partial t^4} \\ &= \frac{q}{EI} - \frac{1}{\mu AG}\frac{\partial^2 q}{\partial z^2} - \frac{2\Omega\rho i}{\mu EAG}\frac{\partial q}{\partial t} + \frac{\rho}{\mu EAG}\frac{\partial^2 q}{\partial t^2} - \frac{1}{EI}\frac{\partial m}{\partial z} \end{aligned} \tag{7}$$

The Timoshenko beam-axle model is divided into two parts, AO and OB, by a circular disk. A rigid disk is fixed at the point of the axis, simplified as a concentrated mass (m_{D}) and concentrated moments of inertia (J_{p} and J_{d}). Assuming that the degrees and angles of the two beam axes are r_1, θ_1, r_2, and θ_2, the free vortex differential equation of the beam axis obtained from Equation (7) is:

$$\frac{\partial^4 r_j}{\partial z_j^4} - \frac{\rho_j}{E_j}\left(1 + \frac{E_j}{\mu_j G_j}\right)\frac{\partial^4 r_j}{\partial z_j^2\,\partial t^2} + \frac{2\Omega\rho_j i}{E_j}\frac{\partial^3 r_j}{\partial z_j^2\,\partial t} + \frac{\rho_j A_j}{E_j I_j}\frac{\partial^2 r_j}{\partial t^2} - \frac{2\Omega\rho_j^2 i}{\mu_j E_j G_j}\frac{\partial^3 r_j}{\partial t^3} + \frac{\rho_j^2}{E_j\mu_j G_j}\frac{\partial^4 r_j}{\partial t^4} = 0 \tag{8}$$

In the formula, j=1,2, $z_j \in [0, l_j]$, where l_j is the length of each segment.

If we only consider the synchronous vortices of the Timoshenko beam-axis model, we can let $r_j = f_j(x)e^{i\omega t}$, and substituting Equation (8), we get:

$$\frac{\mathrm{d}^4 f_j}{\mathrm{d}z_j^4} + \frac{2\gamma_j}{l_j^2}\frac{\mathrm{d}^2 f_j}{\mathrm{d}z_j^2} - \frac{\lambda_j^4}{l_j^4} f_j = 0 \tag{9}$$

$$\frac{2\gamma_j}{l_j^2} = \frac{\rho_j}{E_j}\left(1 + \frac{E_j}{\mu_j G_j}\right)\omega^2 - \frac{2\rho_j\Omega\omega}{E_j} \tag{10}$$

$$\frac{\lambda_j^4}{l_j^4} = \frac{\rho_j A_j}{E_j I_j}\omega^2 + \frac{2\Omega\rho_j^2\omega^2}{\mu_j G_j E_j} - \frac{\rho_j^2\omega^4}{\mu_j G_j E_j} \tag{11}$$

The general solution of Equation (9) is:

$$f_j(x) = c_{j1}\cos\ \alpha_j z_j + c_{j2}\sin\ \alpha_j z_j + c_{j3}\mathrm{ch}\ \beta_j z_j + c_{j4}\mathrm{sh}\ \beta_j z_j \tag{12}$$

Among them:

$$\alpha_j^2 = \frac{\gamma_j + \sqrt{\gamma_j^2 + \lambda_j^4}}{l_j^2}, \beta_j^2 = \frac{-\gamma_j + \sqrt{\gamma_j^2 + \lambda_j^4}}{l_j^2} \tag{13}$$

Similarly, consideration is given to the synchronous vortices of the Timoshenko beam-axis model. For a uniform cross-section rotor, the cross-sectional parameters are independent of z. Assuming $\theta_j = \Theta_j(x)e^{i\omega t}$, it is substituted into Equation (6), and based on the principle of conservation of energy and variational principle, we can obtain:

$$\begin{gathered}\Theta_j' = f''_j + \frac{\omega^2\rho_j}{\mu_j G_j} f_j \\ \Theta_j = \frac{\left(\mu_j G_j A_j + E_j I_j \frac{\omega^2\rho_j}{\mu_j G_j}\right) f_j' + E_j I_j f_j''}{\mu_j G_j A_j - \rho_j I_j \omega^2 + 2\rho_j I_j \Omega\omega}\end{gathered} \tag{14}$$

All boundary conditions and the boundary condition at point O are:

$$\begin{gathered}\mu_2 G_2 A_2(\Theta_2 - f_2')|_{z_2=0} - \mu_1 G_1 A_1(\Theta_1 - f_1')|_{z_1=l_1} = m_\mathrm{D}\omega^2 f_2|_{z_2=0} \\ E_1 I_1 \Theta|_{z_1=l_1} - E_2 I_2 \Theta_2'|_{z_2=0} = \left(J_\mathrm{d}\omega^2\Theta_2 - J_\mathrm{p}\Omega\omega\Theta_2\right)\big|_{z_2=0}\end{gathered} \tag{15}$$

It is noted that the effect of the rigid disk on the rotor vortex is reflected in the boundary condition at point 0.

$$\begin{gathered}f_1|_{z_1=l_1} = f_2|_{z_2=0} \\ \Theta_1|_{z_1=l_1} = \Theta_2|_{z_2=0}\end{gathered} \tag{16}$$

The boundary conditions at point A are:

$$\begin{gathered}\left.\frac{\partial\Theta_1}{\partial z_1}\right|_{z_1=0} = 0 \\ -\mu_1 G_1 A_1(\Theta_1 - f_1')|_{z_1=0} = k_1 f_1|_{z_1=0}\end{gathered} \tag{17}$$

The boundary conditions at point B are:

$$\begin{gathered}\left.\frac{\partial\Theta_2}{\partial z_2}\right|_{z_2=l_2} = 0 \\ \mu_2 G_2 A_2(\Theta_2 - f_2')|_{z_2=l_2} = k_2 f_2|_{z_2=l_2}\end{gathered} \tag{18}$$

where k_1 and k_2 are the stiffness coefficient of the support at the end of axis A and the end of axis B, respectively. The following example demonstrates how to solve the whirling of a segmented continuous mass-spring shaft with a concentrated mass disk.

3 Finite Element Analysis

First, the basic dynamic unbalance response of the rotor system model is simulated using the "Beam Rotor" module in COMSOL Multiphysics 6.0. The "Beam Rotor" interface is often used for structural analysis of rotating mechanical components. Balance equations are typically established in a fixed reference frame. The interface automatically analyzes the gyroscopic moment due to the rotor rotation. The interface uses Timoshenko elements, supports geometric linear analysis, and provides multiple bearing models, including journal bearings, thrust bearings, and active magnetic bearings.

The system spindle length, i.e., the span between the two bearings, is 0.8m. A rigid thin circular plate is mounted in the center of the span. The axis segment of the rotor system is defined by a line segment (edge), and the parameters of the bearings, the plate, and the load are defined by nodes, as shown in Table 1.

Table 1. Parameters of the rotor system model

Parameters of the rotor system model	
Disc density	7850 kg/m^3
Disc eccentricity	1.00E-04 m
Disc outer diameter	0.28 m
Disc thickness	0.07 m
Bearing radial stiffness	1.00E+06
Bearing radial damping coefficient	100
Rotational speed	50 Hz
Shaft length	0.8 m
Shaft diameter	0.05 m
Disc eccentric angle	0
Disc mass	32.757 kg
Disc polar moment of inertia	0.33125 kg*m^2
Disc diameter moment of inertia	0.179 kg*m^2

The shaft of 0.8 meter is divided into four shaft segments, with a total of five nodes. The rotor beam rotor model and the rotor system model are shown in Fig. 2. The main shaft is a solid cylindrical shaft of uniform cross section, with a diameter of 0.05 m and a length of 0.8 m. We set "shaft journal bearings" at nodes 1 and 5, with the bearing support direction along the z-axis. In this model, the effect of gravity is ignored. The bearing model is defined using the "total spring and damping constant." The bearing damping coefficient *Cu* is 100 N*s/m, and the radial stiffness coefficient *Kr* is 1*10^6 N/m. Considering that the connection is rigid and fixed in practical applications, fixed support is chosen as the bearing base. Setting the "disk" at node 3, as in the "beam rotor," the "disk" does not set specific 3D models through geometric modules, and the disk type can be selected as non-circular or circular. When selecting a non-circular disk, the defined parameters of the disk are moment of inertia and mass, indicating that the inertia force of the disk directly affects the rotor system. In this simulation, the "disk" is selected as a circular shape, defined by geometric dimensions, with a density of 7850 kg/m^3, a diameter of 0.28 m, and a thickness of 0.07m. According to the calculation, its

mass is 32.757 kg, the moment of inertia is 0.179 kg*m^2, and the disk is set with an eccentricity of 1e-4 to simulate the unbalanced quantity in the rotor system during rotation. The polar moment of inertia is 0.33125 kg*m^2. The grid division is adopted with edge division.

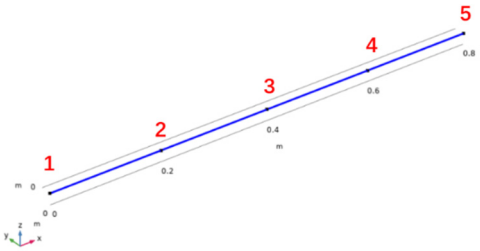

Fig. 2. Finite element model of rotor system

4 Results and Discussion

4.1 Dynamic Analysis of a Fixed Speed Non-Eccentric Single-Span Rotor System

Before studying eccentric rotor systems, a simulation analysis was conducted for a typical non-eccentric single-span rotor system. In comparison to eccentric rotor systems, the disc eccentricity is 0 in the non-eccentric rotor system, and other parameters are consistent with those of the eccentric rotor system. Modal and time-domain analyses were conducted for the rotor system. Two point probes are set at node 1 to monitor the y and z direction vibrations at the bearing point. The simulation parameters are shown in Table 2.

Table 2. Simulation parameters of a fixed speed non-eccentric single-span rotor system

Simulation parameters	
Disc eccentricity	0
Speed	3000 rpm
Acceleration time	0.8 m
Rotary shaft length	0.05 m
Rotary shaft diameter	32.757 kg
Output time	10 s

Fig. 3 shows the vortex situation of the first-order modal of the unbiased single-span turntable rotor system, and Fig. 4 shows the vibration situation at the bearing location (node 1) of the non-eccentric rotor system. In an ideal unbiased state, the displacement at the bearing is zero. When the shaft of the rotor system is not deformed, the centerline of the shaft is coincident with the line connecting the hinges at both ends of the shaft. When the rotor system is isolated from gravity and operates undisturbed, such as in a state of static equilibrium, the axis of the shaft will consistently remain vertical.

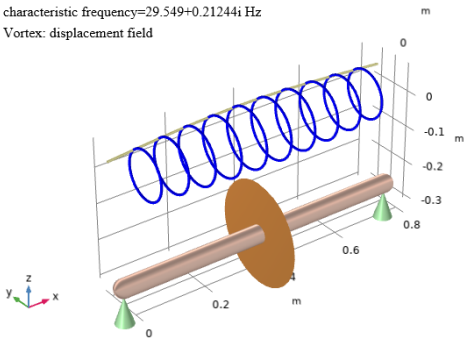

Fig. 3. Vortexing analysis of a single-span rotor system without eccentricity at a constant speed

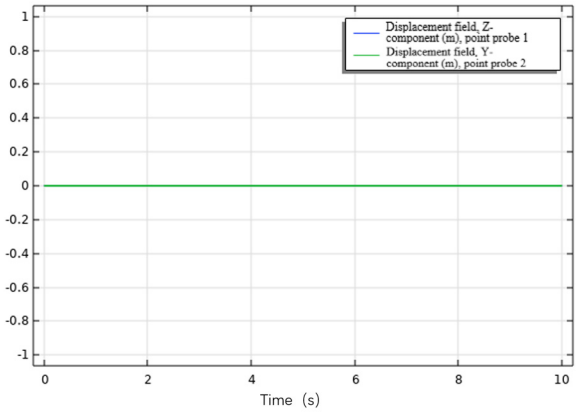

Fig. 4. Vibration at the bearing (node 1)

As shown in Fig. 5, the Campbell diagram for the unbiased single-span turntable rotor system ranges from 0 to 6000 rpm. The Campbell diagram is a commonly used analytical tool in rotor dynamics, where the vibration amplitude at detection points is plotted as a function of rotational speed and frequency, thus showing the full range of changes in the rotor vibration characteristics over the entire rotational speed range. In the Campbell diagram, the horizontal axis represents the speed, and the vertical axis represents the frequency. The forced vibration part, i.e., the frequency component related to the speed, is presented on the ray originating from the origin. The dotted lines in the figure represent the effect of rotor vortices on the natural frequency of the rotor system, and the intersection points of the rays with the dotted lines indicate the resonance points where the rotor's self-rotation and precession coincide, which are the critical speeds. The dotted line corresponding to the rotor speed represents the corresponding frequency of each mode at the current rotor speed. From Fig. 5, it can be seen that the first two-order critical speeds of the unbiased single-span turntable rotor system are 1773 rpm and 4734 rpm, and the first three natural frequencies of the rotor system at 3000 rpm are 29.55 Hz, 84.84 Hz, and 107.62 Hz. According to the frequency domain

analysis of the non-eccentric single-span turntable rotor system, as shown in Fig. 6, there is no obvious line spectrum characteristic in the vibration of the rotor system in the y and z directions. The time-domain vibration situation at the bearing monitored by the probe in the figure is consistent.

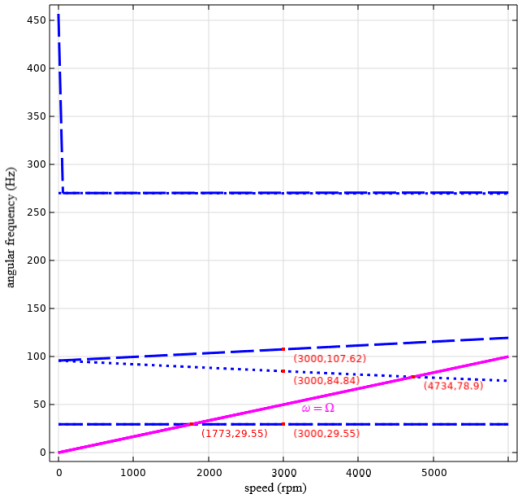

Fig. 5. Campbell diagram of 0-6000rpm for a single-span turntable rotor system without eccentricity

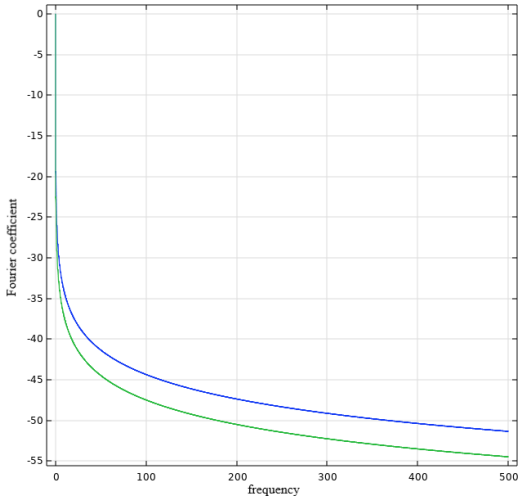

Fig. 6. Frequency domain analysis of a single-span turntable rotor system without eccentricity

4.2 Dynamic Analysis of Constant-Speed Eccentric Single-Span Rotor System

This section analyzes the dynamic characteristics of eccentric single-span turntable rotor systems and explores the research on main control methods for eccentric rotor systems with static imbalance. The simulation parameters are shown in Table 3.

Table 3. Simulation parameters of a constant speed eccentric single-span rotor system

Simulation parameters	
Disc eccentricity	1e-4 m
Speed	3000 rpm
Acceleration time	0.8 m
Rotary shaft length	0.05 m
Rotary shaft diameter	32.757 kg
Output time	10 s

Fig. 7 shows the vortex situation of the eccentric single-span turntable rotor system in the first-order modal state, while Figs. 8-9 show the vibration situation at the bearing location (node 1) of the eccentric rotor system. Compared to the non-eccentric rotor system, there is a significant vibration in the y and z directions at the bearing position with the addition of the rotor eccentricity. The initial rotor system speed is 3000 rpm. The y-direction vibration amplitude of the rotor system is approximately 15e-5m within the first four seconds, and the z-direction vibration amplitude is approximately 20e-5m. This is caused by the inertial force resulting from the initial rotor system vibration in the centrifugal position. Four seconds later, the vibrations of the rotor system gradually stabilized, with the vibration amplitudes in the y and z directions approximately being around 9e-5 meters.

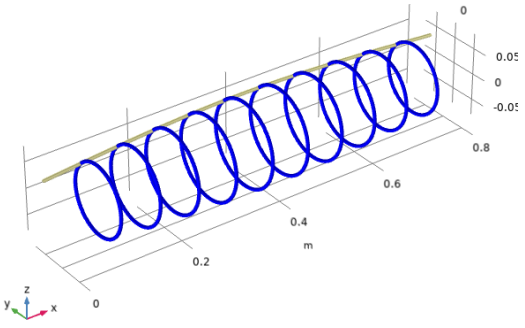

Fig. 7. Vortex analysis of rotor system

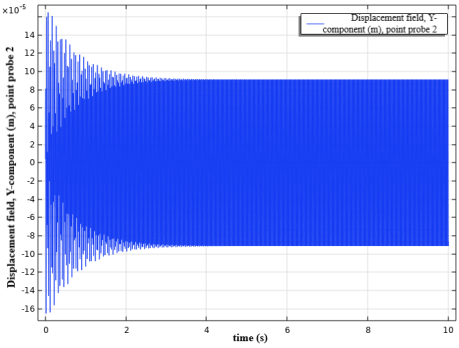

Fig. 8. Displacement in the *y*-direction at the bearing

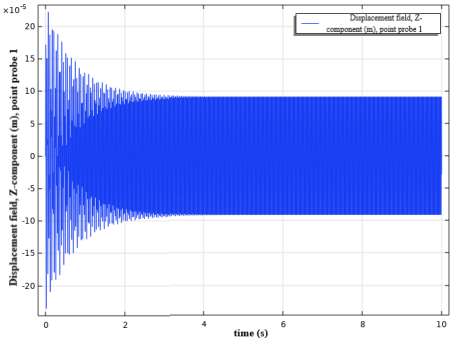

Fig. 9. Displacement in the *z*-direction at the bearing

The vibration of the rotor in 6s-6.2s is shown in Fig. 10. It can be observed from the figure that the vibration amplitudes in both directions are identical, and the phase difference between the vibrations is always pi/2. Under the condition of constant speed for long-term operation of the rotor system, the rotating state always tends to stability.

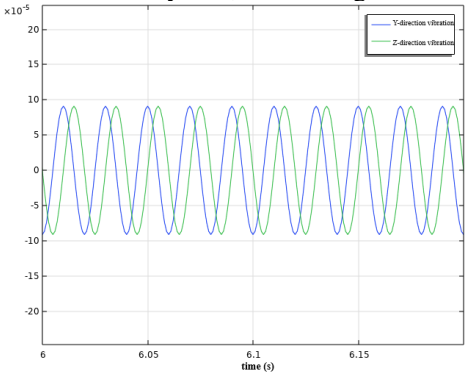

Fig. 10. Vibration of the rotor in 6-6.2 s

Fig. 11 illustrates the Campbell diagram of an eccentric single-span rotor system. In comparison to the non-eccentric rotor system, the natural frequency displayed in the Campbell diagram remains unchanged at 3000 rpm. The eccentricity is considered to be only 1e-4 m, which is relatively small in relation to the rotor system itself and has a minimal impact on the vortex motion of the rotor system.

The frequency domain analysis of the eccentric single-span turntable rotor system is shown in Fig. 12. Within the range of 0-500 Hz, there are two distinct spectral lines on the rotor, located at approximately 29.55 Hz and 50 Hz. The first spectral line is clearly associated with the first-order modal natural frequency of the rotor system as described in the Campbell diagram, while the second spectral line corresponds to the rotor system's rotational frequency at 50 Hz. Compared to the ideal unbiased single-span rotor system, the vibration of the eccentric rotor system is significantly related to the modal and natural frequency of the rotor system.

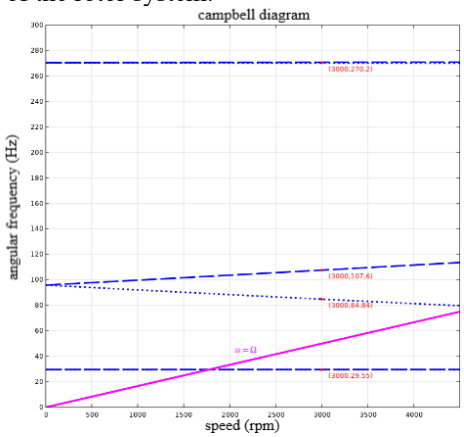

Fig. 11. Campbell diagram of a constant-speed eccentric single-span rotor system

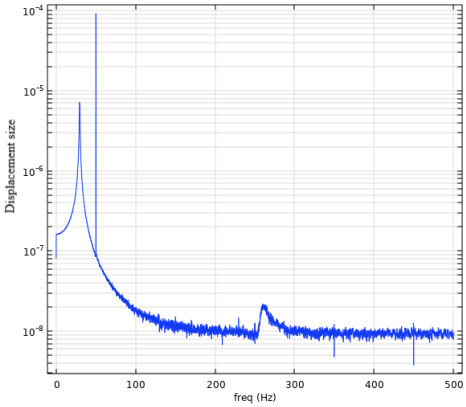

Fig. 12. Frequency domain analysis of eccentric single-span turntable rotor system

4.3 Dynamic Analysis of Accelerated Eccentric Single-Span Rotor System

When considering the effects of rotor vortices, the natural frequency of the rotor system changes with the rotor speed. The natural frequency will vary at different speeds, and when the rotor speed matches the natural frequency, resonance occurs. This specific rotor speed is referred to as the critical speed. Therefore, when calculating the rotor system, different rotational speeds will correspond to different frequencies. One of the primary research focuses on rotor active control is the utilization of active control intervention to modify the rotor modes, allowing for safe passage through critical speeds during acceleration without encountering resonance. Therefore, it is crucial to investigate the dynamic characteristics of eccentric rotor systems under acceleration conditions.

Based on the eccentric single-span rotor system in Section 3.2, a dynamic analysis of rotor acceleration was conducted, with the rotor speed increasing linearly from 0 to 3000 rpm in 100 seconds. The simulation parameters are shown in Table 4:

Table 4. Simulation parameters of an accelerated eccentric single-span rotor system

Simulation parameters	
Disc eccentricity	1e-4 m
Speed	0-3000 rpm
Acceleration time	100 s
Rotary shaft length	0.8 m
Rotary shaft diameter	0.05 m
Disk mass	32.757 kg

As shown in Fig. 13, the z-component displacement at the bearing of an accelerated eccentric single-span rotor system when the speed linearly increases from 0 to 3000 rpm within 0-100 s. At approximately 59.3 to 59.6 seconds, the vibration situation of the rotor system deteriorates significantly, with the maximum amplitude of the z-component displacement approaching 0.003 meters. According to the Campbell diagram of the eccentric rotor system mentioned above, the first critical speed of the rotor system is about 1774 rpm. According to the conversion, the corresponding rotor speed at 59.3s-59.6s is about 1779 rpm-1788 rpm, which is close to the first critical speed. Therefore, it confirms that resonance between the precession and rotation of the rotor system near the critical speed will lead to a deterioration of the vibration situation of the rotor system.

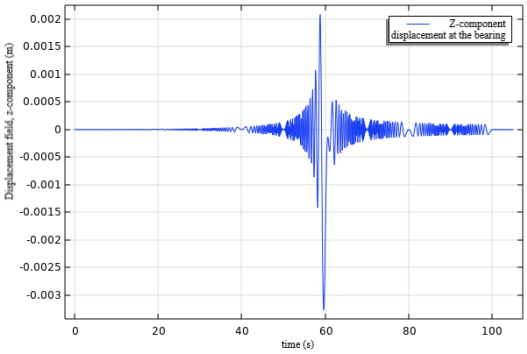

Fig. 13. Acceleration of the Z-component displacement at the bearing of an eccentric single-span rotor system

5 Conclusions

This paper conducts a dynamic analysis of single-span rotor systems based on COMSOL Multiphysics finite element software. The dynamic characteristics of single-span rotor systems with constant speed without eccentricity, constant speed with eccentricity, and accelerated eccentricity are analyzed separately, and the following conclusions are mainly obtained:

1. Within the frequency range of 0-500 Hz, the constant-speed eccentric rotor exhibits two distinct line spectra, located around 29.55 Hz and 50 Hz, respectively. The first line spectrum is clearly consistent with the first-order modal natural frequency of the rotor system as described in the Campbell diagram. In contrast, the second line spectrum corresponds to the rotor system's rotational frequency at 50 Hz. Compared to the ideal unbiased single-span rotor system, the vibration of the eccentric rotor system is significantly related to the modal and natural frequency of the rotor system.
2. As the eccentric rotor system approaches its critical speed, it will experience a resonance between self-rotation and precession, causing a significant increase in the amplitude of the rotor system vibrations. The use of active control technology to dynamically adjust the modal characteristics of the rotor system for stable acceleration has engineering value.

References

1. Wang L.C., Wang A. L., Yin Y. J., et al. Vibration characteristics of complex aero-engine rotors considering support constraints[J]. Journal of Aerospace Power, 2023, 38(04): 901-912.
2. Zhou S. T., Guo W. N., Xiao Q, et al. Vibration characteristics analysis of emu traction motor rotor under eccentric faults[J]. Engineering Mechanics, 2021, 38(07): 216-225.

3. Yang S. H., Hu Y., Xiao Z. H., et al. Rotor vibration analysis of large-scale centrifugal compressor under the flexible support[J]. Journal of Mechanical Engineering, 2019, 55(19): 121-127.
4. Feng Y., Wang J. D., Han D. J. Experimental study on rotor vibration characteristics of high speed turbine generators [J]. Noise and Vibration Control, 2019, 39(04): 95-100.
5. Zuo S. G., Liu J. F., Wu X. D., et al. Analysis on vibration characteristics of vehicle centrifugal fan rotor system[J]. Transactions of the Chinese Society of Agricultural Engineering, 2016, 32(04):84-90.
6. Xiang L., Wang Z. R., Tang G. J. Nonlinear dynamic analysis for unbalanced rotor-bearing-seal systems[J]. Journal of North China Electric Power University (Natural Science Edition), 2012, 39(05): 59-64.
7. Zhu L., Wei D. G., Shi W. Effects of eccentricity on rotor dynamics characteristic of turbocharger[J]. Chinese Journal of Automotive Engineering, 2013, 3(04): 282-286.
8. Yuan X. P., Xu W. B., Li B. Study on dynamic performance of rotor system considering the mass eccentricity[J]. Mechanical Research & Application, 2017, 30(01): 80-82.